Journal Pre-proof

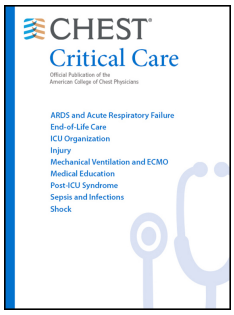

Superimposed Pressure Predicts Mortality in Acute Respiratory Failure during Spontaneous Breathing: insights from the CT-COVID19 multicenter study group.

Emanuele Rezoagli, Davide Signori, Yi Xin, Sarah Gerard, Aurora Magliocca, Francesca Graziano, Giovanni Vitale, Linda Mussoni, Jonathan Montomoli, Matteo Subert, Alessandra Ponti, Savino Spadaro, Giancarla Poli, Francesco Casola, Roberta Garberi, Davide Raimondi Cominesi, Alice Nova, Marco Giani, Giuseppe Foti, John Laffey, Maurizio Cereda, for the CT-COVID19 Multicenter Study Group

PII: S2949-7884(25)00104-2

DOI: https://doi.org/10.1016/j.chstcc.2025.100231

Reference: CHSTCC 100231

To appear in: *CHEST Critical Care*

Received Date: 26 June 2025

Revised Date: 3 November 2025

Accepted Date: 10 November 2025

Please cite this article as: Rezoagli E, Signori D, Xin Y, Gerard S, Magliocca A, Graziano F, Vitale G, Mussoni L, Montomoli J, Subert M, Ponti A, Spadaro S, Poli G, Casola F, Garberi R, Cominesi DR, Nova A, Giani M, Foti G, Laffey J, Cereda M, for the CT-COVID19 Multicenter Study Group, Superimposed Pressure Predicts Mortality in Acute Respiratory Failure during Spontaneous Breathing: insights from the CT-COVID19 multicenter study group., *CHEST Critical Care* (2026), doi: https://doi.org/10.1016/j.chstcc.2025.100231.

Word count abstract: 296
Word count text: 3458

Title: Superimposed Pressure Predicts Mortality in Acute Respiratory Failure during Spontaneous Breathing: insights from the CT-COVID19 multicenter study group.

Running head: Superimposed Pressure predicts mortality in respiratory failure during spontaneous breathing

Authors

Emanuele Rezoagli*[1,2], Davide Signori[3], Yi Xin[4,5], Sarah Gerard[6], Aurora Magliocca[7,8], Francesca Graziano,[1,9], Giovanni Vitale[7], Linda Mussoni[10], Jonathan Montomoli[11,12], Matteo Subert[13], Alessandra Ponti[14], Savino Spadaro[15,16], Giancarla Poli[17], Francesco Casola[18,19], Roberta Garberi[1,2], Davide Raimondi Cominesi[1,2], Alice Nova[1,2], Marco Giani[1,2], Giuseppe Foti[1,2], John Laffey[20,21], Maurizio Cereda[4,5] for the CT-COVID19 Multicenter Study Group

CT-COVID19 multicenter study group collaborators:

Department of Anaesthesia and Critical Care Medicine & Department of Radiology, Papa Giovanni XXIII Hospital, Bergamo, Italy*: Matteo Cazzaniga, Ferdinando Luca Lorini & Pietro Bonaffini*;
Department of Translational Medicine, University of Ferrara, Ferrara, Italy*: Irene Ottaviani*;
Department of Anesthesiology and Intensive Care, ASST Lecco, Lecco, Italy*: Asia Borgo, Mario Tavola*;
Department of Anesthesia and Intensive Care Medicine, Melzo-Gorgonzola Hospital, Azienda Socio-Sanitaria Territoriale Melegnano e della Martesana, Melegnano, Milan, Italy*: Livio Ferraris*;
Department of Emergency and Intensive Care, & Department of Radiology, Fondazione IRCCS San Gerardo dei Tintori Hospital, Monza, Italy*: Giacomo Bellani, Stefano Gatti, Andrea Restivo, Filippo Serra & Davide Ippolito*;
Istituto per la Sicurezza Sociale, San Marino, San Marino*: Massimo Arlotti, Marino Gatti, Beatrice Tamagnini*;
Department of Anesthesia and Intensive Care, Infermi Hospital, AUSL Romagna, Rimini, Italy*: Enrico Cavagna, Emiliano Gamberini*;
Department of Anesthesia and Intensive Care Medicine, Policlinico San Marco, Gruppo Ospedaliero San Donato, Bergamo, Italy*: Davide De Ponti, Giuseppe Galbiati, Matteo Giacomini*.

Author Affiliations

[1]School of Medicine and Surgery, University of Milano-Bicocca, Monza, Italy
[2]Department of Emergency and Intensive Care, Fondazione IRCCS San Gerardo dei Tintori Hospital, Monza, Italy
[3]Department of Anesthesia and Intensive Care, ASST-Bergamoest, Seriate, Italy
[4]Department of Anesthesiology, Critical Care, and Pain Medicine, Massachusetts General Hospital, Harvard Medical School, Boston, USA
[5]Department of Anesthesiology and Critical Care, University of Pennsylvania, Philadelphia, USA

[6]Roy J. Carver Department of Biomedical Engineering, University of Iowa, Iowa City, IA, USA
[7]Department of Anesthesia and Intensive Care Medicine, Policlinico San Marco, Gruppo Ospedaliero San Donato, Bergamo, Italy
[8]Department of Pathophysiology and Transplantation, University of Milan, Milan, Italy
[9]Biostatistics and Clinical Epidemiology, Fondazione IRCCS San Gerardo dei Tintori, Monza, Italy
[10]Istituto per la Sicurezza Sociale, San Marino, San Marino
[11]Department of Anesthesia and Intensive Care, Infermi Hospital, AUSL Romagna, Rimini, Italy
[12]Health Services Research, Evaluation and Policy Unit, Romagna Local Health Authority, Viale Settembrini 2, Rimini 47923, Italy
[13]Department of Anesthesia and Intensive Care Medicine, Melzo-Gorgonzola Hospital, Azienda Socio-Sanitaria Territoriale Melegnano e della Martesana, Melegnano, Milan, Italy
[14]Department of Anesthesiology and Intensive Care, ASST Lecco, Lecco, Italy
[15]Anesthesia and Intensive Care, Azienda Ospedaliero-Universitaria of Ferrara, Ferrara, Italy
[16]Department of Translational Medicine, University of Ferrara, Ferrara, Italy
[17]Department of Anaesthesia and Critical Care Medicine, Papa Giovanni XXIII Hospital, Bergamo, Italy
[18]Department of Physics, Harvard University, 17 Oxford St., Cambridge, MA 02138, USA
[19]Harvard-Smithsonian Centre for Astrophysics, 60 Garden St., Cambridge, MA 02138, USA
[20]School of Medicine, National University of Ireland Galway, Galway, Ireland
[21]Department of Anaesthesia and Intensive Care Medicine, Galway University Hospitals, Galway, Ireland

***Corresponding author:**

Emanuele Rezoagli, MD, PhD
School of Medicine and Surgery, University of Milano-Bicocca, Monza, Italy
Email: emanuele.rezoagli@unimib.it
Phone: +39 039 2339273

Conflict of Interest

The authors declare no competing interests.

Source of support

This study was funded by Institutional funds. E.R. was supported by the Bicocca Starting grant 2020 from the University of Milano-Bicocca with the project titled: “Functional Residual Capacity Assessment using a Wash-In/Wash-Out technique based on a fast main-stream O2 Sensor with nanofluorescenT geometry for severe lung injury (FAST)—COVID and beyond”.

Author contributions

E.R. conceived the study and supervised the study project, provided clinical laboratory and computed tomography data, analyzed data, interpreted data, searched literature, wrote the manuscript and is the coordinator of the multicenter clinical study; D.S. analyzed data,

interpreted data, searched literature, and wrote the manuscript; Y.X. analyzed computed tomography data by manual segmentation, interpreted data and revised the manuscript; S.G. performed deep learning analysis of computed tomography data, interpreted data and revised the manuscript; A.M., G.V., L.M., J.M., M.S., A.P., S.S. and G.P. provided clinical laboratory and computed tomography data, interpreted data, and revised the manuscript; F.C. provided logistical management of computed tomography data, interpreted data and revised the manuscript; R.G., D.R.C., A.N., M.G., G.F. and J.G.L. interpreted data and revised the manuscript; M.C. coordinated the data analysis of the lung CT data, interpreted data and revised the manuscript. All authors gave final approval of the version to be published and agreed to be accountable for all aspects of the work in ensuring that questions related to the accuracy and integrity of any part of the work are appropriately investigated and resolved.

Ethical consideration and data acquisition

The study was performed under the Declaration of Helsinki and in agreement with the Italian good clinical practice recommendations (D.M. Sanità del 15/07/97 e s.m.i.) and with the applied healthcare hospital protocols, as we previously described (1). No change of current clinical practice or clinical protocols in use were taken in place in the enrolled study population. Considering the retrospective nature of the proposed study, we did not anticipate risks nor benefits that might be added to the patients. Moreover, in the presence of technical difficulties related to the emergency health context to obtain an informed consent from patients in that period of pandemic, informed con- sent was waived. For this reason and for the great public interest of the project, the research was conducted in the context of the authorizations guaranteed by Article 89 of the GDPR EU Regulation 2016/679, which guarantees the treatment for purposes of public interest, scientific or historical research or for statistical purposes of health data. Personal data were handled in compliance with the European Regulation on the Protection of Personal Data (GDPR), the Legislative Decree 196/2003 and subsequent amendments and additions, and any other Italian law applicable to the protection of personal data (henceforth referred to as the “applicable data protection law”). Data were collected in a pseudo-anonymous way through paper case report forms, digitalized on a University of Milano-Bicocca Institutional Google drive account and analyzed by the scientific coordinator of the project (E.R.). Favorable judgment for the execution of the study was obtained before data acquisition from the local institutional review board of the coordinating center Fondazione IRCCS San Gerardo dei Tintori, Monza, Italy (Approval date: 24/04/2020; number 3375) and from the local institutional review board of each enrolled center (Policlinico San Marco, Gruppo Ospedaliero San Donato, Zingonia, Bergamo, Italy; Ospedale Infermi, Rimini, Italy; Ospedale Papa Giovanni XXIII, Bergamo, Italy; Ospedale Alessandro Manzoni, Lecco, Italy; Arcispedale Sant’Anna, Ferrara, Italy; Ospedale Santa Maria delle Stelle, Melzo, Italy; Istituto Sicureza Sociale, Repubblica di San Marino).
Baseline characteristics (age, sex, body mass index, comorbidities) and clinical illness severity (Sequential Organ Failure Assessment (SOFA) and pH) were collected, together with laboratory biomarkers, blood gas analysis, respiratory assistance, and hemodynamic data at hospital admission. Lung CT scans acquired for clinical purposes within the first week since hospital admission were obtained. Data on drug treatments and complications during hospital admissions, outcomes including length of stay (in ICU and in hospital), use of non-invasive respiratory support, mechanical ventilation-free days, limitation of life sustaining measures, ICU mortality, and hospital mortality were recorded.

References

1. Rezoagli E, Xin Y, Signori D, Sun W, Gerard S, Delucchi KL, et al. Phenotyping COVID-19 respiratory failure in spontaneously breathing patients with AI on lung CT-scan. Crit Care Lond Engl. 2024 Aug 5;28(1):263.

Word count abstract: 296
Word count text: 3458

Title: Superimposed Pressure Predicts Mortality in Acute Respiratory Failure during Spontaneous Breathing: insights from the CT-COVID19 multicenter study group.

Running head: Superimposed Pressure predicts mortality in respiratory failure during spontaneous breathing

Abbreviation List

AHRF = acute hypoxemic respiratory failure
AIC = Akaike information criterion
ANOVA = analysis of variance
ARDS = acute respiratory distress syndrome
ARF = acute respiratory failure
AUROC = area under the receiving operating characteristics
BIC = Bayesian information criterion
BMI = body mass index
CI = confidence interval
COPD = chronic obstructive pulmonary disease
CNN = convolutional neural network
CT = computed tomography
FiO_2 = inspiratory oxygen fraction
GGO = ground glass opacity
HU = Hounsfield Unit
ICU = intensive care unit
IQR = interquartile range
LA = left apical
LB = left basal
LOS = length of stay
$PaCO_2$ = arterial carbon dioxide partial pressure
PaO_2 = arterial oxygen partial pressure
pH = negative logarithm of hydrogen concentration
RA = right apical
RB = right basal
ROI = region of interest
SD = standard deviation
SOFA = sequential organ failure assessment

Abstract

Background: Early lung imaging may improve patient management and prognostication in acute respiratory failure.
Research question: We aimed to explore whether quantitative assessment of lung injury by computed tomography (CT) predicts outcome in spontaneously breathing patients with COVID-19 acute respiratory failure.
Study Design and Methods: This is a large retrospective, multicenter, cohort study including patients presenting to the Emergency Department with a clinical diagnosis of COVID-19 respiratory failure and undergoing early lung CT scan at hospital admission. Lung injury was characterized by the severity of lung involvement as follows: 1) absence, unilateral, or bilateral infiltrates; 2) number of lung quadrants affected by infiltrates (0-4); level of global and regional 3) superimposed pressure (SP) and 4) gas/tissue ratio (G/T). Baseline, laboratory and clinical characteristics were described by the presence or absence of laterality of lung infiltrates. Association of 90-day mortality and lung CT characterization was explored using Cox multivariable models and areas under receiving operating characteristics. Subphenotypes including CT assessment were explored by latent class analyses.
Results: Eight-hundred and eight patients were included. Bilateral infiltrates were associated with higher global and regional SP and G/T and a higher 90-day mortality (38%) compared with unilateral infiltrates (18%) or no lung infiltrates (11%). Involvement by laterality, quadrants, degree of global SP and G/T were all associated with the degree of hypoxemia on admission and 90-day mortality. Among other CT-derived variables of lung injury, SP characterized a subphenotype with a robust relationship with 90-day mortality.
Interpretation: Characterization of lung injury severity by early lung CT describes the severity of hypoxemia. The adjunct of CT global SP to clinical and laboratory parameters identified a subphenotype with high 90-day mortality prediction. Early lung CT may enhance population enrichment and improve prognostication in non-intubated patients with acute respiratory failure.
Trial registration: clinicaltrials.gov Identifier: NCT04395482.

Keywords: computed tomography; superimposed pressure; respiratory failure; COVID-19; artificial intelligence; mortality; spontaneous breathing.

Computed tomography (CT) of the lungs is of paramount importance in the clinical and physiological characterization of lung injury in patients with acute hypoxemic respiratory failure (AHRF) (1,2). CT informed pathophysiological constructs of the more severe AHRF phenotype, the acute respiratory distress syndrome (ARDS), including the “baby lung” (3) and the “sponge lung” models (4). Furthermore, CT quantitatively (5) and qualitatively (6) described the severity of lung injury. Recently, lung CT helped separate heterogeneous populations of critically ill patients into distinct subgroups (7,8), showing potential in improving prognostication(9) and personalization of therapeutic interventions (10), particularly in ARDS (11). Population enrichment by lung CT seems a valid option to better phenotype patients with respiratory failure (12) and target precision medicine endpoints (13,14).

Quantitative CT analysis can extract a number of candidate imaging features, but it is unclear which of these variables can best summarize injury characteristics when screening large image datasets. In patients with ARDS, CT quantification of the superimposed pressure (SP) and gas to tissue ratio (G/T) described the degree of lung injury during passive ventilation (1). SP estimates the compressive forces that, due to inflammatory pulmonary edema, cause dependent lung collapse, and requires relatively straightforward image processing. G/T described the balance between the gas versus the tissue content in the lungs, suggesting a decreased alveolar gas content or an increased tissue content in the presence of a decreased G/T value. (1, 15,16). However, no clinical investigation reported correlations between SP values and G/T and clinical outcomes. Recently, in a secondary analysis of the LUNG SAFE study, Pham et al. (17) characterized lung injury according to its laterality (unilateral versus bilateral) and the number of quadrants involved by lung infiltrates on chest X-ray lung images, reporting independent correlations between radiological distribution and mortality. This approach requires simple processing and is similar to that adopted to score chest X-ray films in the formulation of the lung injury score (LIS) by Murray et al. (18).

The majority of studies assessing lung injury through CT were conducted in mechanically ventilated patients with ARDS (9,19,20). In comparison, the role of CT in the characterization of the broader population of spontaneously breathing patients with AHRF is underexplored. In a large CT-COVID19 multicenter dataset, we showed that integrating quantitative CT characteristics with clinical variables separated two phenotypes of non-ventilated COVID-19-related AHRF (12). In the current study, we further expanded this study population to test the hypothesis that lung CT measurements of pulmonary SP, G/T and morphological distribution of lung infiltrates according to laterality and quadrant involvement may have associations with lung injury severity–according to oxygenation criteria–and may enrich the prediction of clinical outcomes during spontaneous breathing.

Materials and Methods

Ethical consideration and data acquisition

The study was performed under the Declaration of Helsinki and in agreement with the Italian good clinical practice recommendations (.M. Sanità del 15/07/97 e s.m.i.) and with the applied healthcare hospital protocols, as we previously described (12).

Inclusion and exclusion criteria

Clinical, laboratory and CT data were collected between February and April 2020, during the peak of the first Italian wave of the COVID-19 pandemic.

Inclusion criteria:

1. Patients≥18 years;
2. Positive confirmation of SARS-CoV-2 infection with nucleic acid amplification test or serology of SARS-CoV2 by nasopharyngeal swab, broncho-aspirate sample or bronchoalveolar lavage;
3. Lung CT scan performed within 7 days since hospital admission.

All patients included in the current analysis were admitted to the Emergency Department with a clinical diagnosis of respiratory failure.

Exclusion criteria:

1. Patients undergoing mechanical ventilation during CT acquisition;
2. Patients with CT data that cannot be used to estimate CT derived parameters as SP.

Chest CT quantification

The lung CT images were collected, anonymized, and sent by the University of Milano-Bicocca Institutional Google drive account to the University of Pennsylvania, Department of Anesthesiology and Critical Care, and Department of Radiology (M.C., Y.X., and S.G.) in a de-identified format for advanced quantitative analysis. CT images were segmented using a previously validated convolutional neural network(CNN) (21,22). After segmentation, whole-lung and lobar lung masks were inspected by a trained investigator (Y.X.), and manually adjusted using ITK-snap software (23). SP and G/T were calculated as follows:

- global SP (24) and global G/T (1);
- apical to basal-regional SP and G/T: by dividing the lung in 10 equally distributed sections from the apical to the basal trajectory (25);
- ventral to dorsal-regional SP and G/T: by dividing the lung into 10 equally gravitationally distributed sections.

Specifically, we defined as a lung infiltrate any investigated ROI with a mean lung CT density≥-750 HU, as per previous reported thresholds in COVID-19 lesions (i.e. ground glass opacification (26) and high-opacity consolidation regions (27–29). The population was then stratified based on the laterality of the lungs involved by infiltrates (i.e. none, unilateral, and bilateral) and by the number of affected quadrants (i.e. 0,1,2,3, and 4). Finally, global SP and G/T were analyzed as continuous data and categorized into tertiles for time to event prognostication.

Statistical analysis

Continuous variables were expressed as mean and standard deviation (SD) and median and interquartile range (IQR), while categorical variables were summarized as absolute and relative frequencies. Group comparisons were performed using the chi-square or Fisher's exact test for categorical variables, and one-way analysis of variance (ANOVA). P-values were adjusted for multiple testing using the Benjamini–Hochberg procedure. Differences in 90-days mortality were assessed by Kaplan–Meier survival analyses and by univariable and multivariable Cox proportional regression models. We applied latent class analysis (LCA) including both clinical and CT-derived variables to explore distinct subphenotypes, and their association with mortality. Multivariable and predictive models were adjusted for clinically relevant covariates (demographics (i.e. age, sex); any comorbidities; non-respiratory SOFA score (i.e. composed of renal, hepatic and coagulation components); severity of lung injury by oxygenation criteria (PaO_2/FiO_2); inflammatory activation (i.e. white blood cells); metabolism (i.e. arterial pH). All analyses were performed using R software.

Extensive description of materials and methods was detailed in the Online Supplemental material.

Results

Patient population

A total of 853 patients were initially screened, of whom 808 patients met inclusion criteria for the current analysis. CT scans were obtained at a median 0 days (IQR 0;0) since hospital admission. Among them-according to the criteria chosen for the presence of lung infiltrates-214 patients (26.5%) had no CT-based lung involvement, 85 patients (10.5%) had unilateral CT-based infiltrates, and 509 patients (63.0%) had bilateral CT-based infiltrates (**eTable 1** and **eFigure1)**.

Baseline Characteristics

We summarized baseline characteristics, comorbidities, and clinical illness severity at hospital admission, stratified by groups with different laterality of lung involvement (CT density≥-750 HU) in **Table1** and **eTable1**. As compared with no or unilateral infiltrate, patients with bilateral infiltrates were older, had higher inflammatory biomarkers and platelet count. Further, patients with bilateral infiltrates had a higher prevalence of endothelial dysfunction risk factors such as chronic kidney disease, diabetes and systemic hypertension. On hospital admission, both hypoxemia and requirement for oxygen administration were worse in patients with bilateral infiltrates than in the other two groups.

Quantitative and Qualitative Analysis of Lung CT Images

We provide a comprehensive analysis of quantitative and qualitative lung CT parameters stratified by laterality groups. Measurements were obtained in the whole lung, in the left and in the right lung (**Table2**), and in the 4 lung quadrants (**eTable2)**. As compared with patients with no or unilateral infiltrates, patients with bilateral infiltrates had higher mean lung density, lung mass and the lowest lung volume across all examined ROIs and quadrants. Further, they had a higher proportion of tissue involved by lung injury, including both ground glass opacities and lung consolidation.

Among all CT-derived continuous variables, we explored global and regional characterization of global SP and G/T as they showed the strongest association with 90-day mortality by time AUROC (**eTable 3**).

SP and G/T

We described the levels of global SP and G/T across increasing lung injury severity by laterality and quadrants of injury (Figure 1) and at a regional level (Figure 2 and eFigure 3).

Regional SP increased from ventral to dorsal and from apical to basal thoracic sections, linearly and with an inverse U-shape, respectively. G/T gradually decreased from ventral to dorsal and from apical to basal thoracic sections (**Figure 2A,B and eFigure 3A,B**). Regional SP and G/T were higher and lower, respectively, across all the thoracic sections over increasing degrees of lung injury assessed by lung laterality and number of quadrants (**Figure 2C-F and eFigure 2C-F**).
In **eFigure 2**, global SP and G/T are separately displayed for both the right and the left lung and stratified according to laterality (**A,B**) and to number of quadrants (**C,D**) involved by lung infiltrates. In patients with unilateral infiltrates, comparing right-sided versus left-

sided injury, right-sided lungs trended toward a higher global SP. This was observed also in patients with bilateral infiltrates and across increasing number of injured quadrants (**A,B**). G/T was lower in the right versus left lung in the presence of 3 injured quadrants but no difference was observed across lung laterality of injury (**C,D**).

Gas exchange parameters

We reported the associations between lung injury involvement by CT and gas exchange parameters in **Figure3.** Patients with bilateral infiltrates had the lowest PaO_2/FiO_2 ratio(220±100 mmHg), followed by those with unilateral infiltrates (272±85 mmHg) and no infiltrates(334±82 mmHg; p<0.001) (**Figure3A**). Patients with 4 injured lung quadrants had the lowest PaO_2/FiO_2(200±99 mmHg), while patients with no quadrants involved showed the highest PaO_2/FiO_2(334±82 mmHg; p<0.001) (**Figure3C**). A significant negative correlation was observed between global SP and G/T with oxygenation (R^2=0.302; p<0.001) (**Figure3E, G, eTable4**).
There were no significant differences in $PaCO_2$ levels according to the laterality of lung injury (**Figure3B)**, the number of lung injured quadrants (**Figure3D**) and the degree of global SP and G/T (**Figure3F, H, eTable4**).

Treatments, Complications and Outcomes of Patients Stratified by Lung Involvement

Pharmacological treatments, complications and clinical outcomes of patients stratified by lung laterality are provided in **eTable5.**
Patients with bilateral infiltrates had a significantly longer hospital stay (16±19 days) compared to those with no infiltrates (11±16 days) and unilateral infiltrates (15±14 days; p=0.002). Contrarily, ICU length of stay (LOS) was significantly shorter in patients with bilateral infiltrates (17±15 days) compared to those with unilateral infiltrates (31±25 days) and no infiltrates (28±23 days; p=0.007). Patients with bilateral infiltrates had a significantly higher hospital mortality rate (38%) compared to those with unilateral infiltrates (18%) and no infiltrates (11%; p<0.001).

Time-to-event analyses

Figure 4 presents the Kaplan-Meier survival curves at 90-day follow-up stratified by laterality of lung injury (**A**), number of injured quadrants(**B**) and global SP and G/T categories by tertiles (**C, D**). Survival probability was progressively increasing from bilateral (38%) to unilateral (18%) to absence of lung infiltrates (11%) (Log-rank p<0.001). As the number of affected quadrants increased, the survival probability decreased from 89% (no quadrant involved) to 56% (4 injured quadrants) (Log-rank p<0.001; **B**).
The survival rate was the lowest in patients with the highest tertile of global **SP** (50%) and the highest in those with the lowest tertile (86%) (Log-rank p<0.001; **C**). Contrarily, survival rate was the lowest in patients with the lowest tertile of global G/T (51.3%) and the highest in those with the highest tertile (87.4%) (Log-rank p<0.001; **D**).

We tested whether the association of the CT-derived variables of lung injury severity with 90-day mortality may add to the prediction model fitting of a multivariable model including major clinically meaningful covariates (**Table 3**).

Only global SP and G/T were independently associated with 90-day mortality, showing the best-fit adjusted Cox proportional regression models for predicting 90-day mortality with

the lowest Akaike Information Criterion and Bayesian Information Criterion (**model B,C**). These findings were confirmed after implementing multiple imputations to the multivariable models **(eTable6).**

Latent class analyses

We applied latent class analyses to explore whether distinct subphenotypes including the CT-derived study variables could improve the association with 90-day mortality. Graphical representation of subphenotypes identified by LCA are reported in **eFigure4**. Subphenotypes identified by adding global SP to the core dataset unveiled the more robust association with 90-day mortality as shown by the lower AIC 2346 and BIC 2349, and the higher concordance of 0.68 (SE=0.20) as compared to the other explored models (**Table 4**).

Discussion

We conducted a large retrospective multicenter observational cohort study including more than 800 patients spontaneously breathing with COVID-19 respiratory failure who underwent lung CT scan at hospital admission. In this population, we report the following key findings:

- Patients with bilateral infiltrates on chest CT had higher mean lung density, larger lung mass, and lower lung gas volume as compared with patients with no or unilateral infiltrates;
- Dissemination of lung infiltrates according to laterality or number of quadrants was associated with more severe hypoxemia, higher global and regional SP, and a lower global and regional G/T;
- Survival probability decreased over laterality involvement, number of injured quadrants, and global superimposed pressure and G/T values;
- Lung injury severity by laterality, number of quadrants, and degree of global SP and G/T predicted 90-day mortality;
- SP and G/T independently predicted 90-day mortality after adjustments for clinically meaningful covariates and outperformed a multivariable model without including computed tomography lung injury assessment;
- Subphenotypes of injury identified by LCA highlighted that - among the CT-derived study variables - superimposed pressure showed the best fitting model of association with 90-day mortality.

We showed that CT characterization of lung injury severity has a role in outcome prediction in spontaneously breathing patients with acute hypoxemic respiratory failure. Among the tested CT-derived variables, global SP had the best accuracy in predicting mortality, as compared to topographic injury dissemination, laterality and G/T.

In this large multicenter cohort of patients with COVID-19 respiratory failure we observed that characterization of lung injury by chest CT according to the laterality of lung infiltrates identified different clinical, laboratory and outcome descriptors. Our analysis unveiled significant differences in baseline characteristics, comorbidities, and clinical illness severity between patients with no lung infiltrates, unilateral infiltrates, and bilateral infiltrates. Bilateral lung infiltrates were associated with older age, higher levels of systemic inflammation, a higher proportion of comorbidities, and worse clinical outcomes. As patients with bilateral infiltrates had significantly higher levels of inflammatory biomarkers, this finding may suggest an early acute inflammatory response at hospital admission which could be useful in predicting treatment responses (30–32).

Our findings are in line with those reported by Pham and colleagues, who observed baseline clinical and outcome differences between patients with ARDS versus patients with unilateral infiltrates (17) as visually identified on chest X-ray. Furthermore, our results add to their data because we confirm association between lung injury severity by laterality and number of quadrants with mortality in a different population of spontaneously breathing patients with COVID-19 acute respiratory failure. While Pham et al. performed their radiological assessment on plain chest X-ray, we observed that global SP, which can only be obtained via quantitative CT, was the more robust predictor of mortality.

SP and G/T had a pivotal role in the characterization of lung injury severity in ARDS and in the understanding of the effects of ventilator setting during passive ventilation (33), since

the early '90s, with the studies by Gattinoni and coworkers (4,34). However, no studies explored whether SP and G/T may associate with outcome in patients with respiratory failure and during spontaneous breathing. Our data suggest that–as for lung injury severity assessed by lung laterality and number of quadrants–global SP and G/T strongly correlated with the degree of hypoxemia, considered by most an index of severity of respiratory failure. This finding is in line with the data by Pelosi et al. who highlighted a higher SP in the presence of acute respiratory failure (i.e. lower oxygenation because of a lower gas to tissue ratio) as compared to normal subjects (i.e. higher oxygenation because of a higher gas to tissue ratio (34). Interestingly, $PaCO_2$ levels did not significantly differ over increasing lung injury severity as assessed by lung laterality, number of injured quadrants of degree of SP. We can speculate that in spontaneously breathing patients who were studied early after hospital admission, the CO_2 was probably controlled by patients' relatively preserved respiratory drive.

Interestingly, bilateral infiltrates were associated with increased total lung injury, because of a higher proportion of both ground-glass opacities (GGO) and consolidation. Consequently, the global and regional SP was higher as compared with patients with unilateral or with no infiltrates. As the lung height did not relevantly change across the groups, the differences in SP suggested that the change in lung density is the primary marker characterizing the severity of pulmonary edema due to lung injury. In fact, SP values increase in the presence of an injured lung (i.e. higher density and lower lung gas volume).

After adjustment for clinically meaningful variables, SP and G/T improved outcome prognostication as compared to a multivariable model including only oxygenation as a marker of lung injury severity. Furthemore, when explored by LCA, the identification of subphenotypes including CT-derived variables showed that SP allowed to obtain the highest association with 90-day mortality. This further emphasizes the importance of the mechanical increase of weight of the lungs because of injury and edema, and its potential as a target to optimize therapeutic strategies. Different quantitative and qualitative lung CT variables were explored to improve population enrichment strategies and better characterize specific clusters of patients and add to patient prognostication (12,35,36). However, considering its comprehensive role in integrating different dimensions of lung injury including lung height as a proxy of lung geometry and lung density as a descriptor of the balance between gas and lung tissue content - the role of SP may better characterize heterogeneous populations with respiratory failure that may respond differently to pharmacological treatment (37) or ventilator setting (38). Finally, superimposed pressure is a quantitative variable that can be rapidly obtained within the radiological CT assessment, and its quantification can be automatized once gravimetric and volumetric information are obtained.

Incorporating early CT data alongside clinical and laboratory parameters using latent class analysis appears to facilitate the identification of subphenotypes with strong mortality-predictive value. This suggests that early quantitative lung CT could be a valuable tool for predictive enrichment and prognostication in non-intubated patients with acute respiratory failure. Although the AI-assisted lung segmentation technique is highly accurate—requiring manual correction in only 3% of CT studies—the prognostic benefit of early lung CT should be weighed against the patient's overall clinical stability, including hemodynamic and neurological integrity, to ensure safe imaging.

Our study has some strengths. First, it includes a homogeneous cohort of spontaneously breathing patients with respiratory failure enrolled during the same COVID-19 pandemic wave, limiting genetic Sars-CoV2 genetic variation and potential preventative measures (e.g. vaccines). Second, it is a large multicenter cohort study including more than 800 patients undergoing early lung CT-scan at hospital admission and during spontaneous breathing. Third, our analysis on lung injury severity took advantage of an advanced validated algorithm for lung segmentation of the region of interest explored at the lung CT by convolutional neural network that were later manually confirmed (22). Fourth, this study explores for the first time the role of SP, G/T, lung laterality and injured quadrants on the characterization by lung injury severity (i.e. gas exchange) and prognostication (i.e. 90-day mortality) in spontaneously breathing patients. This is relevant reminding that the prognostication role of SP was not yet investigated during passive ventilation. Fifth, SP is easily quantifiable by a software and this procedure may be automatized and immediately provide this key diagnostic and prognostic information immediately after the acquisition of the CT images.

While our study provides valuable insights, it has some limitations. The retrospective design and the lack of standardized imaging protocols across centers may introduce variability in CT data acquisition. The assessment of SP by lung computed tomography in non-intubated patients has not been previously validated; therefore, our findings should be interpreted as exploratory and hypothesis-generating. Further, lung CT did not include vascular phases. However, although in a limited sample size no differences in Dimers were observed between degrees of injury severity across lung laterality. We acknowledge that our study focuses on patients with COVID-19-related acute respiratory failure, therefore these findings may not be generalizable to other causes of hypoxemic respiratory failure. However, this ensures a highly homogeneous study population which can be considered a critically ill model of viral pneumonia, reducing variability, and allowing a robust physiological, imaging and outcome characterization. Finally, while arterial carbon dioxide elimination was recorded, data on patient respiratory drive and minute ventilation were not available because the patients were not intubated.

Conclusions

In conclusion, our study highlights the importance of early lung CT imaging in the characterization of lung injury severity in spontaneously breathing patients with COVID-19 induced acute respiratory failure. Lung injury severity described by laterality or quadrants of lung infiltrates and global SP and G/T strongly correlates with the degree of hypoxemia. In our multicenter cohort, SP identifies a subphenotype of injury which is strongly associated with 90-day mortality and may play a critical role in population enrichment and outcome prognostication.

References

1. Gattinoni L, Caironi P, Pelosi P, Goodman LR. What has computed tomography taught us about the acute respiratory distress syndrome? Am J Respir Crit Care Med. 2001 Nov 1;164(9):1701–11.

2. Rouby JJ, Puybasset L, Nieszkowska A, Lu Q. Acute respiratory distress syndrome: lessons from computed tomography of the whole lung. Crit Care Med. 2003 Apr;31(4 Suppl):S285-295.

3. Gattinoni L, Pesenti A. The concept of “baby lung.” Intensive Care Med. 2005 June 1;31(6):776–84.

4. Gattinoni L, Pelosi P, Vitale G, Pesenti A, D’Andrea L, Mascheroni D. Body Position Changes Redistribute Lung Computed-Tomographic Density in Patients with Acute Respiratory Failure. Anesthesiology. 1991 Jan 1;74(1):15.

5. Cressoni M, Gallazzi E, Chiurazzi C, Marino A, Brioni M, Menga F, et al. Limits of normality of quantitative thoracic CT analysis. Crit Care Lond Engl. 2013 May 24;17(3):R93.

6. Gattinoni L, Pesenti A, Torresin A, Baglioni S, Rivolta M, Rossi F, et al. Adult respiratory distress syndrome profiles by computed tomography. J Thorac Imaging. 1986 July;1(3):25–30.

7. Goodman LR, Fumagalli R, Tagliabue P, Tagliabue M, Ferrario M, Gattinoni L, et al. Adult Respiratory Distress Syndrome Due to Pulmonary and Extrapulmonary Causes: CT, Clinical, and Functional Correlations. Radiology. 1999 Nov;213(2):545–52.

8. Mrozek S, Jabaudon M, Jaber S, Paugam-Burtz C, Lefrant JY, Rouby JJ, et al. Elevated Plasma Levels of sRAGE Are Associated With Nonfocal CT-Based Lung Imaging in Patients With ARDS: A Prospective Multicenter Study. Chest. 2016 Nov;150(5):998–1007.

9. Rouby JJ, Puybasset L, Cluzel P, Richecoeur J, Lu Q, Grenier P, et al. Regional distribution of gas and tissue in acute respiratory distress syndrome. II. Physiological correlations and definition of an ARDS Severity Score. Intensive Care Med. 2000 Aug 1;26(8):1046–56.

10. Constantin JM, Jabaudon M, Lefrant JY, Jaber S, Quenot JP, Langeron O, et al. Personalised mechanical ventilation tailored to lung morphology versus low positive end-expiratory pressure for patients with acute respiratory distress syndrome in France (the LIVE study): a multicentre, single-blind, randomised controlled trial. Lancet Respir Med. 2019 Oct;7(10):870–80.

11. Rezoagli E, Fumagalli R, Bellani G. Definition and epidemiology of acute respiratory distress syndrome. Ann Transl Med. 2017 July;5(14):282.

12. Rezoagli E, Xin Y, Signori D, Sun W, Gerard S, Delucchi KL, et al. Phenotyping COVID-19 respiratory failure in spontaneously breathing patients with AI on lung CT-scan. Crit Care Lond Engl. 2024 Aug 5;28(1):263.

13. Filippini DFL, Di Gennaro E, van Amstel RBE, Beenen LFM, Grasso S, Pisani L, et al. Latent class analysis of imaging and clinical respiratory parameters from patients with COVID-19-related ARDS identifies recruitment subphenotypes. Crit Care. 2022 Nov 25;26(1):363.

14. Nishikimi M, Ohshimo S, Bellani G, Fukumoto W, Anzai T, Liu K, et al. Identification of novel sub-phenotypes of severe ARDS requiring ECMO using latent class analysis. Crit Care. 2024 Oct 24;28(1):343.

15. Gattinoni L, Pesenti A, Baglioni S, Vitale G, Rivolta M, Pelosi P. Inflammatory pulmonary edema and positive end-expiratory pressure: correlations between imaging and physiologic studies. J Thorac Imaging. 1988 July;3(3):59–64.

16. Gattinoni L, D'Andrea L, Pelosi P, Vitale G, Pesenti A, Fumagalli R. Regional Effects and Mechanism of Positive End-Expiratory Pressure in Early Adult Respiratory Distress Syndrome. JAMA. 1993 Apr 28;269(16):2122–7.

17. Pham T, Pesenti A, Bellani G, Rubenfeld G, Fan E, Bugedo G, et al. Outcome of acute hypoxaemic respiratory failure: insights from the LUNG SAFE Study. Eur Respir J. 2021 June 10;57(6).

18. Murray JF, Matthay MA, Luce JM, Flick MR. An Expanded Definition of the Adult Respiratory Distress Syndrome. Am Rev Respir Dis. 1988 Sept;138(3):720–3.

19. Gattinoni L, Cressoni M. Quantitative CT in ARDS: towards a clinical tool? Intensive Care Med. 2010 Nov 1;36(11):1803–4.

20. Bitker L, Talmor D, Richard JC. Imaging the acute respiratory distress syndrome: past, present and future. Intensive Care Med. 2022;48(8):995–1008.

21. Gerard SE, Herrmann J, Kaczka DW, Musch G, Fernandez-Bustamante A, Reinhardt JM. Multi-resolution convolutional neural networks for fully automated segmentation of acutely injured lungs in multiple species. Med Image Anal. 2020 Feb;60:101592.

22. Gerard SE, Herrmann J, Xin Y, Martin KT, Rezoagli E, Ippolito D, et al. CT image segmentation for inflamed and fibrotic lungs using a multi-resolution convolutional neural network. Sci Rep. 2021 Jan 14;11(1):1455.

23. Yushkevich PA, Piven J, Hazlett HC, Smith RG, Ho S, Gee JC, et al. User-guided 3D active contour segmentation of anatomical structures: significantly improved efficiency and reliability. NeuroImage. 2006 July 1;31(3):1116–28.

24. Nova A, Xin Y, Victor M, Gaulton TG, Alcala GC, Winkler T, et al. Biomechanical implications of mass loading in a swine model of acute hypoxemic respiratory failure. J Appl Physiol. 2025 Sept;139(3):849–62.

25. Spina S, Mantz L, Xin Y, Moscho DC, Ribeiro De Santis Santiago R, Grassi L, et al. The pleural gradient does not reflect the superimposed pressure in patients with class III obesity. Crit Care Lond Engl. 2024 Sept 16;28(1):306.

26. Chaganti S, Grenier P, Balachandran A, Chabin G, Cohen S, Flohr T, et al. Automated Quantification of CT Patterns Associated with COVID-19 from Chest CT. Radiol Artif Intell. 2020 July;2(4):e200048.

27. Mergen V, Kobe A, Blüthgen C, Euler A, Flohr T, Frauenfelder T, et al. Deep learning for automatic quantification of lung abnormalities in COVID-19 patients: First experience and correlation with clinical parameters. Eur J Radiol Open. 2020;7.

28. Gong K, Wu D, Arru CD, Homayounieh F, Neumark N, Guan J, et al. A multi-center study of COVID-19 patient prognosis using deep learning-based CT image analysis and electronic health records. Eur J Radiol. 2021 June 1;139:109583.

29. Mader C, Bernatz S, Michalik S, Koch V, Martin SS, Mahmoudi S, et al. Quantification of COVID-19 Opacities on Chest CT - Evaluation of a Fully Automatic AI-approach to Noninvasively Differentiate Critical Versus Noncritical Patients. Acad Radiol. 2021 Aug;28(8):1048–57.

30. Famous KR, Delucchi K, Ware LB, Kangelaris KN, Liu KD, Thompson BT, et al. Acute Respiratory Distress Syndrome Subphenotypes Respond Differently to Randomized Fluid Management Strategy. Am J Respir Crit Care Med. 2017 Feb;195(3):331–8.

31. Calfee CS, Delucchi KL, Sinha P, Matthay MA, Hackett J, Shankar-Hari M, et al. Acute respiratory distress syndrome subphenotypes and differential response to simvastatin: secondary analysis of a randomised controlled trial. Lancet Respir Med. 2018 Sept 1;6(9):691–8.

32. Maddali MV, Churpek M, Pham T, Rezoagli E, Zhuo H, Zhao W, et al. Validation and utility of ARDS subphenotypes identified by machine-learning models using clinical data: an observational, multicohort, retrospective analysis. Lancet Respir Med. 2022 Apr 1;10(4):367–77.

33. Cressoni M, Chiumello D, Carlesso E, Chiurazzi C, Amini M, Brioni M, et al. Compressive forces and computed tomography-derived positive end-expiratory pressure in acute respiratory distress syndrome. Anesthesiology. 2014 Sept;121(3):572–81.

34. Pelosi P, D'Andrea L, Vitale G, Pesenti A, Gattinoni L. Vertical gradient of regional lung inflation in adult respiratory distress syndrome. Am J Respir Crit Care Med. 1994 Jan;149(1):8–13.

35. Ball L, Robba C, Herrmann J, Gerard SE, Xin Y, Pigati M, et al. Early versus late intubation in COVID-19 patients failing helmet CPAP: A quantitative computed tomography study. Respir Physiol Neurobiol. 2022 July;301:103889.

36. Gattinoni L, Chiumello D, Caironi P, Busana M, Romitti F, Brazzi L, et al. COVID-19 pneumonia: different respiratory treatments for different phenotypes? Intensive Care Med. 2020 June;46(6):1099–102.

37. Horie S, McNicholas B, Rezoagli E, Pham T, Curley G, McAuley D, et al. Emerging pharmacological therapies for ARDS: COVID-19 and beyond. Intensive Care Med. 2020 Dec;46(12):2265–83.

38. Wendel-Garcia PD, Moser A, Jeitziner MM, Aguirre-Bermeo H, Arias-Sanchez P, Apolo J, et al. Dynamics of disease characteristics and clinical management of critically ill COVID-19 patients over the time course of the pandemic: an analysis of the prospective, international, multicentre RISC-19-ICU registry. Crit Care. 2022 July 4;26(1):199.

39. Raschke RA, Agarwal S, Rangan P, Heise CW, Curry SC. Discriminant Accuracy of the SOFA Score for Determining the Probable Mortality of Patients With COVID-19 Pneumonia Requiring Mechanical Ventilation. JAMA. 2021 Apr 13;325(14):1469–70.

40. Rezoagli E, McNicholas B, Pham T, Bellani G, Laffey JG. Lung-kidney cross-talk in the critically ill: insights from the Lung Safe study. Intensive Care Med. 2020 May;46(5):1072–3.

41. McNicholas BA, Rezoagli E, Simpkin AJ, Khanna S, Suen JY, Yeung P, et al. Epidemiology and outcomes of early-onset AKI in COVID-19-related ARDS in comparison with non-COVID-19-related ARDS: insights from two prospective global cohort studies. Crit Care. 2023 Jan 5;27(1):3.

42. Rezoagli E, McNicholas BA, Madotto F, Pham T, Bellani G, Laffey JG, et al. Presence of comorbidities alters management and worsens outcome of patients with acute respiratory distress syndrome: insights from the LUNG SAFE study. Ann Intensive Care. 2022 May 21;12(1):42.

Figure legends

Figure 1. Relationship between lung involvement, SP and Gas/Tissue ratio (G/T). (**A–B**) Comparison of SP (**A**) and Gas/Tissue ratio (**B**) across categories of lung infiltrates (none, unilateral, bilateral). (**C–D**) Comparison of SP (**C**) and Gas/Tissue ratio (**D**) according to the number of lung quadrants involved with disease (n, ≥-750 HU). Bars represent mean values ± standard deviation. p-values refer to one-way ANOVA comparisons. n=808 patients.

Figure 2. Thoracic profiles of regional lung density (dorsal to ventral) and SP. (A–B) Overall profiles of regional SP (cmH_2O) and Gas/Tissue ratio across 10 thoracic sections from dorsal to ventral regions (n = 808). (C–D) SP (cmH_2O) and Gas/Tissue ratio categorized by CT-based lung involvement according to laterality: None (n = 214), Unilateral (n = 85), Bilateral (n = 509). (E–F) SP (cmH_2O) and Gas/Tissue ratio categorized by the number of quadrants with disease: 0 quadrants (n = 214), 1 quadrant (n = 66), 2 quadrants (n = 107), 3 quadrants (n = 95), 4 quadrants (n = 326). Changes of SP (A) and Gas/Tissue ratio (B) across dorsal to ventral regions of the lungs were significantly different ($p<0.05$, repeated measurements one-way ANOVA). Each dot represents the mean value of each thoracic section. Vertical bars indicate ± 1 standard deviation. Asterisks indicate sections with statistically significant differences between groups ($p<0.05$, one-way ANOVA).

Figure 3. Comparison of gas exchange parameters and their association with lung involvement. (**A–B**) PaO_2/FiO_2 and $PaCO_2$ values stratified by the extent of lung infiltrates (none, unilateral, bilateral). (**C–D**) PaO_2/FiO_2 and $PaCO_2$ values across increasing number of injured lung quadrants (n, ≥-750 HU). (**E–F**) Linear correlation between global SP with PaO_2/FiO_2 (**E**) and $PaCO_2$ (**F**). Linear correlation between global gas to tissue ratio (whole lung) with PaO_2/FiO_2 (**G**) and $PaCO_2$ (**H**). Bars represent mean values ± 1 standard deviation. p-values refer to ANOVA tests (**A–D**), linear regression analyses between SP with PaO_2/FiO_2 and $PaCO_2$ (**E–F**) and linear regression analysis between gas to tissue ratio with PaO_2/FiO_2 and $PaCO_2$ (**G–H**). The shaded area around the regression lines represents the 95% confidence interval.

Figure 4. Kaplan-Meier survival curves according to lung involvement and SP categories. (A) Survival stratified by CT-based lung infiltrates (none, unilateral, bilateral). (B) Survival according to the number of quadrants involved with disease (n, ≥-750 HU). (C) Survival stratified by tertiles of global SP. Lower tertile range: 2.1-4.6 cmH_2O; middle tertile range: 4.6-6.6 cmH_2O; upper tertile range: 6.6-15.3 cmH_2O. (D) Survival stratified by tertiles of global G/T. Lower tertile range: 0.3–2.0; middle tertile range: 2.0–3.3; upper tertile range: 3.3–7.7. The number of patients at risk at different time points is shown below each graph. The follow-up was censored at 90 days for all patients. All analyses were conducted in the overall cohort of 808 patients.

Take Home Points

Study Question: Does early quantitative assessment of lung injury on computed tomography (CT) predict outcomes in spontaneously breathing patients with COVID-19–related acute respiratory failure?

Results: Among CT-derived metrics used to quantify lung injury, superimposed pressure identified a distinct subphenotype of non-intubated patients with acute respiratory failure. It showed the strongest association with 90-day mortality, outperforming lung laterality, the number of affected quadrants, and the gas-to-tissue ratio.

Interpretations: Early CT-based evaluation of superimposed pressure in non-intubated patients with acute respiratory failure may improve prognostication and support population enrichment in clinical studies.

Table 1. Baseline characteristics, clinical illness severity, comorbidities, and respiratory support at hospital admission stratified by lung involvement (CT density≥-750 HU).

		Overall (N=808)	No infiltrates (N=214)	Unilateral infiltrates (N=85)	Bilateral infiltrates (N=509)	p
Demographic characteristics						
Age (years); N=808		66.6 (14.6)	61.4 (15.1)	67.2 (14.8)	68.7 (13.8)	<0.001
BMI (Kg/m^2); N=326		27.9 (4.8)	27.3 (5.1)	27.1 (4.0)	28.1 (4.8)	0.383
Sex F (%); N=808		35	38	32	35	0.579
Clinical baseline characteristics						
Temperature (°C); N=785		37.6 (1.0)	37.3 (1.0)	37.8 (1.1)	37.7 (1.0)	<0.001
Renal SOFA		0 (0-1)	0 (0-0)	0 (0-0)	0 (0-1)	0.001
Hepatic SOFA		0 (0-0)	0 (0-0)	0 (0-0)	0 (0-0)	0.227
Coagulation SOFA		0 (0-1)	0 (0-1)	0 (0-1)	0 (0-1)	0.190
WBCs (x1000/µL); N=789		7.4 (3.8)	6.1 (2.5)	6.9 (3.5)	8.0 (4.1)	<0.001
PaO_2/FiO_2 (mmHg); N=708		253.5 (105.9)	333.7 (81.5)	272.3 (85.1)	219.7 (99.9)	<0.001
$PaCO_2$ (mmHg); N=707		32.9 (5.6)	32.6 (5.3)	32.7 (6.3)	33.0 (5.6)	0.724
$HCO3^-$ (mmol/l); N=701		22.8 (3.5)	22.6 (3.0)	22.6 (3.5)	22.9 (3.7)	0.465
pH; N=702		7.5 (0.0)	7.5 (0.0)	7.5 (0.1)	7.5 (0.0)	0.855
Major Comorbidities						
COPD; N=808		46 (5.7)	11 (5.1)	4 (4.7)	31 (6.1)	0.808
Asthma; N=808		34 (4.2)	9 (4.2)	4 (4.7)	21 (4.1)	0.970
Congestive heart failure; N=808		35 (4.3)	7 (3.3)	4 (4.7)	24 (4.7)	0.674
Chronic kidney disease; N=808		50 (6.2)	10 (4.7)	1 (1.2)	39 (7.7)	0.040
Chronic liver failure; N=808		5 (0.6)	1 (0.5)	1 (1.2)	3 (0.6)	0.772
Solid cancer; N=808		29 (3.6)	8 (3.7)	4 (4.7)	17 (3.3)	0.814
Hematologic malignancy; N=808		13 (1.6)	3 (1.4)	3 (3.5)	7 (1.4)	0.331
Immune mediated disease; N=808		31 (3.8)	10 (4.7)	1 (1.2)	20 (3.9)	0.359
Diabetes; N=808		134 (16.6)	14 (6.5)	17 (20)	103 (20.2)	<0.001
Systemic hypertension; N=808		401 (49.6)	76 (35.5)	47 (55.3)	278 (54.6)	<0.001
Atrial fibrillation; N=808		77 (9.5)	12 (5.6)	11 (12.9)	54 (10.6)	0.059
Hypothyroidism; N=558		33 (5.9)	5 (5.4)	2 (3.6)	26 (6.3)	0.713
Respiratory support; N=788						<0.001
Oxygen delivery	Room air	521 (66.1)	176 (86.7)	58 (69)	287 (57.3)	
	LFO	250 (31.7)	26 (12.8)	26 (31)	198 (39.5)	
Non-invasive ventilation	cPAP	17 (2.2)	1 (0.5)	0 (0)	16 (3.2)	
Time between admission and CT scan, days; median (IQR); N=784		0 (0;0)	0 (0;0)	0 (0;0)	0 (0;0)	0.986

Table 2. Quantitative and qualitative analysis of lung CT images stratified by lung laterality. Values are expressed as mean (standard deviation).

	Overall (N=808)	No infiltrates (N=214)	Unilateral infiltrates (N=85)	Bilateral infiltrates (N=509)	p
WHOLE LUNG					
Lung density (HU)	-707 (108)	-824 (25)	-770 (22)	-647 (91)	p<0.001
Lung volume (L)	4.07 (1.28)	5.31 (1.09)	4.44 (1.09)	3.49 (0.96)	p<0.001
Lung gas volume (L)	2.96 (1.25)	4.39 (0.98)	3.42 (0.87)	2.29 (0.78)	p<0.001
Gas/tissue ratio	2.89 (1.41)	4.79 (0.88)	3.39 (0.44)	2.00 (0.68)	p<0.001
Lung mass (kg)	1.11 (0.34)	0.92 (0.16)	1.02 (0.25)	1.20 (0.37)	p<0.001
GGO (%)	34.7 (15.8)	16.2 (4.7)	25.6 (5.4)	44.0 (11.7)	p<0.001
Consolidation (%)	6.7 (6.3)	2.3 (0.6)	3.8 (1.5)	9.0 (6.9)	p<0.001
Total injury (%)	41.4 (19.7)	18.5 (5.1)	29.3 (5.4)	53.1 (14.7)	p<0.001
Lung height (cm)	20.0 (2.1)	20.2 (2.0)	20.4 (2.3)	19.8 (2.1)	0.012
Global superimposed pressure (cmH_2O)	5.8 (2.2)	3.6 (0.6)	4.7 (0.7)	7.0 (1.9)	p<0.001
LUNG LATERALITY					
Left lung					
Lung density (HU)	-705 (118)	-823 (27)	-769 (40)	-645 (106)	p<0.001
Lung volume (L)	1.88 (0.63)	2.48 (0.54)	2.04 (0.53)	1.61 (0.48)	p<0.001
Lung gas volume (L)	1.37 (0.61)	2.05 (0.49)	1.58 (0.43)	1.05 (0.40)	p<0.001
Gas/tissue ratio	2.90 (1.44)	4.78 (0.91)	3.45 (0.69)	2.02 (0.75)	p<0.001
Lung mass (kg)	0.51 (0.16)	0.43 (0.08)	0.47 (0.14)	0.55 (0.18)	p<0.001
GGO (%)	35.1 (16.3)	16.6 (5.0)	26.0 (7.1)	44.5 (12.5)	p<0.001
Consolidation (%)	6.8 (7.8)	2.2 (0.6)	3.7 (2.3)	9.2 (8.9)	p<0.001
Total injury (%)	41.9 (20.5)	18.8 (5.4)	29.7 (8.2)	53.7 (16.0)	p<0.001
Lung height (cm)	18.7 (2.9)	19.4 (2.1)	18.9 (3.3)	18.3 (3.0)	p<0.001
Global superimposed pressure (cmH_2O)	5.4 (2.1)	3.4 (0.6)	4.4 (1.1)	6.5 (2.0)	p<0.001
Right lung					
Lung density (HU)	-705 (112)	-824 (27)	-766 (40)	-645 (95)	p<0.001
Lung volume (L)	2.19 (0.68)	2.83 (0.57)	2.40 (0.65)	1.89 (0.51)	p<0.001
Lung gas volume (L)	1.59 (0.67)	2.34 (0.52)	1.85 (0.55)	1.23 (0.42)	p<0.001
Gas/tissue ratio	2.90 (1.46)	4.82 (0.94)	3.39 (0.74)	2.00 (0.71)	p<0.001
Lung mass (kg)	0.60 (0.19)	0.49 (0.09)	0.55 (0.13)	0.65 (0.20)	p<0.001
GGO (%)	34.5 (16.2)	15.9 (5.0)	25.9 (7.7)	43.8 (12.3)	p<0.001
Consolidation (%)	6.9 (6.8)	2.4 (0.8)	4.1 (2.4)	9.3 (7.5)	p<0.001
Total injury (%)	41.4 (20.1)	18.3 (5.4)	29.9 (8.6)	53.1 (15.3)	p<0.001
Lung height (cm)	19.2 (2.9)	19.7 (2.2)	19.3 (3.4)	19.0 (3.0)	0.007
Global superimposed pressure (cmH_2O)	5.6 (2.2)	3.5 (0.6)	4.5 (1.1)	6.7 (2.1)	p<0.001

HU=Hounsfield units; GGO: ground-glass opacities. Adjusted p-value for multiple comparisons was reported according to Benjamini & Hochberg.

Table 3. Multivariable analyses of association between 90-day mortality and CT-derived characterization of lung injury severity adjusted for the core dataset in the complete cases.

Variable	Adjusted HR (95%CI) p-value Model A: Core dataset	Adjusted HR (95%CI) p-value Model B: Core dataset + SP	Adjusted HR (95%CI) p-value Model C: Core dataset + G/T	Adjusted HR (95%CI) p-value Model D: Core dataset + laterality	Adjusted HR (95%CI) p-value Model E: Core dataset + quadrants
Demographic and clinical variables					
Age, n	1.06 (1.04-1.07) p<0.001	1.06 (1.04-1.07) p<0.001	1.06 (1.04-1.07) p<0.001	1.05 (1.04-1.07) p<0.001	1.06 (1.04-1.08) p<0.001
Sex (Ref. Male)	0.65 (0.46-0.90) p=0.010	0.63 (0.45-0.88) p=0.007	0.58 (0.41-0.81) p=0.002	0.63 (0.45-0.88) p=0.007	0.57 (0.40-0.80) p=0.001
Any comorbidities (Ref. No)	1.25 (0.84-1.87) p=0.267	1.19 (0.80-1.78) p=0.389	1.22 (0.82-1.81) p=0.332	1.23 (0.82-1.84) p=0.309	1.22 (0.82-1.81) p=0.337
PaO_2/FiO_2	0.99 (0.99-0.99) P<0.001	0.99 (0.99-0.99) P<0.001	0.99 (0.99-0.99) P<0.001	0.99 (0.99-0.99) P<0.001	0.99 (0.99-0.99) P<0.001
Non-respiratory SOFA	1.30 (1.15-1.48) p<0.001	1.311(1.15-1.48) p<0.001	1.29 (1.14-1.47) p<0.001	1.30 (1.14-1.48) p<0.001	1.30 (1.14-1.48) p<0.001
pH	0.29 (0.02-5.29) p=0.403	0.48 (0.03-8.83) p=0.620	0.38 (0.02-7.03) p=0.514	0.27 (0.01-4.89) p=0.373	0.54 (0.03-10.97) p=0.690
WBC ($x10^3$)	0.99 (0.95-1.05) p=0.470	0.99 (0.95-1.02) p=0.490	0.98 (0.95-1.02) p=0.384	0.99 (0.95-1.02) p=0.407	0.98 (0.95-1.01) p=0.260
CT lung injury severity					
Superimposed pressure (cmH_2O)		1.14 (1.06-1.23) <p=0.001	-	-	
Gas/Tissue ratio (%)			0.76 (0.64-0.90) P<0.001		
Lung infiltrates (Ref. None)					
• Unilateral		-		1.04 (0.49-2.21) p=0.924	
• Bilateral		-		1.40 (0.79-2.48) p=0.253	
Quadrants (Ref. None)					
• One		-	-		1.29 (0.58-2.87) p=0.537
• Two		-	-		0.91 (0.46-1.83) p=0.799
• Three		-	-		1.13 (0.58-2.20) p=0.714
• Four		-	-		1.77 (0.98-3.22) p=0.059
AIC	2197	2187	2188	2199	2194
BIC	2220	2213	2214	2229	2230
Concordance (standard error)	0.827 (0.012)	0.831 (0.012)	0.830 (0.012)	0.828 (0.012)	0.830 (0012)

N=595 Events=199. Missing data for PaO_2/FiO_2 (n=100 – 12.4%), non-respiratory SOFA (n=141 – 17.5%), pH (n=106 – 13.1%), WBC (n=19 – 2.4%).

Table 4. Association between 90-day mortality and subphenotypes through latent class analyses including core dataset and CT-derived characterization of lung injury severity.

LCA	HR (95% CI)	p-value	AIC	BIC	Concordance (SE)
Model A: Core dataset (Ref. S1)	2.19 (1.65-2.91)	<0.001	2440	2442	0.60 (0.02)
Model B: Core dataset + SP (Ref. S1)	5.06 (3.81-6.73)	<0.001	2346	2349	0.68 (0.01)
Model C: Core dataset + G/T (Ref. S1)	2.32 (1.75-3.10)	<0.001	2434	2438	0.60 (0.02)
Model D: Core dataset + Laterality (Ref. S1)	3.61 (2.42-5.38)	<0.001	2417	2420	0.62 (0.01)
Model E: Core dataset + Quadrants (Ref. S1)	4.18 (3.11-5.63)	<0.001	2372	2375	0.67 (0.02)

SP=global superimposed pressure; S1=subphenotype 1; S2=subphenotype 2.

Model A: S1 N=327; S2 N=268
Model B: S1 N=422; S2 N=173
Model C: S1 N=298; S2 N=297
Model D: S1 N=400; S2 N=195
Model E: S1 N=361; S2 N=234

Figure 1.

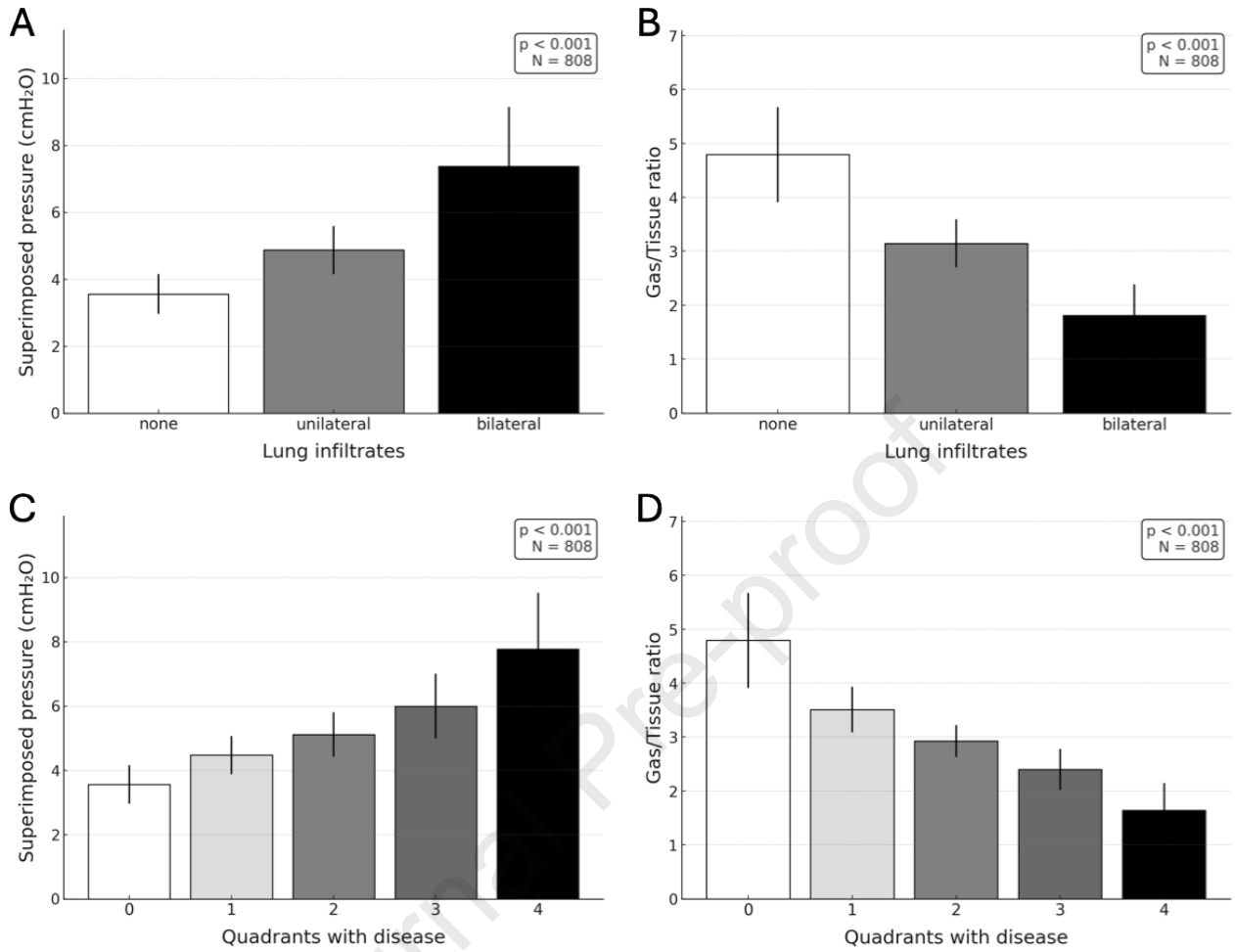

Figure 2.

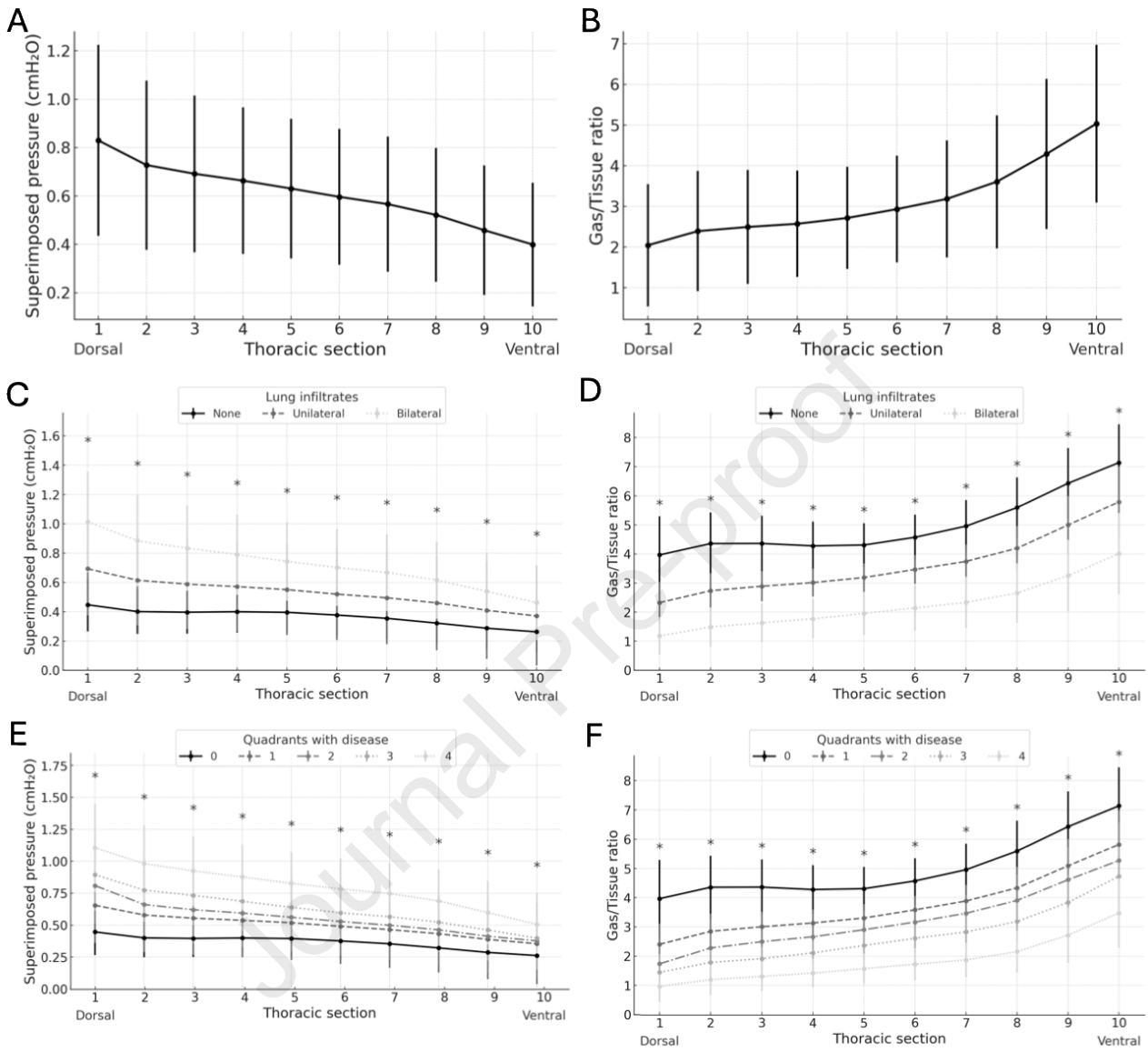

Figure 3.

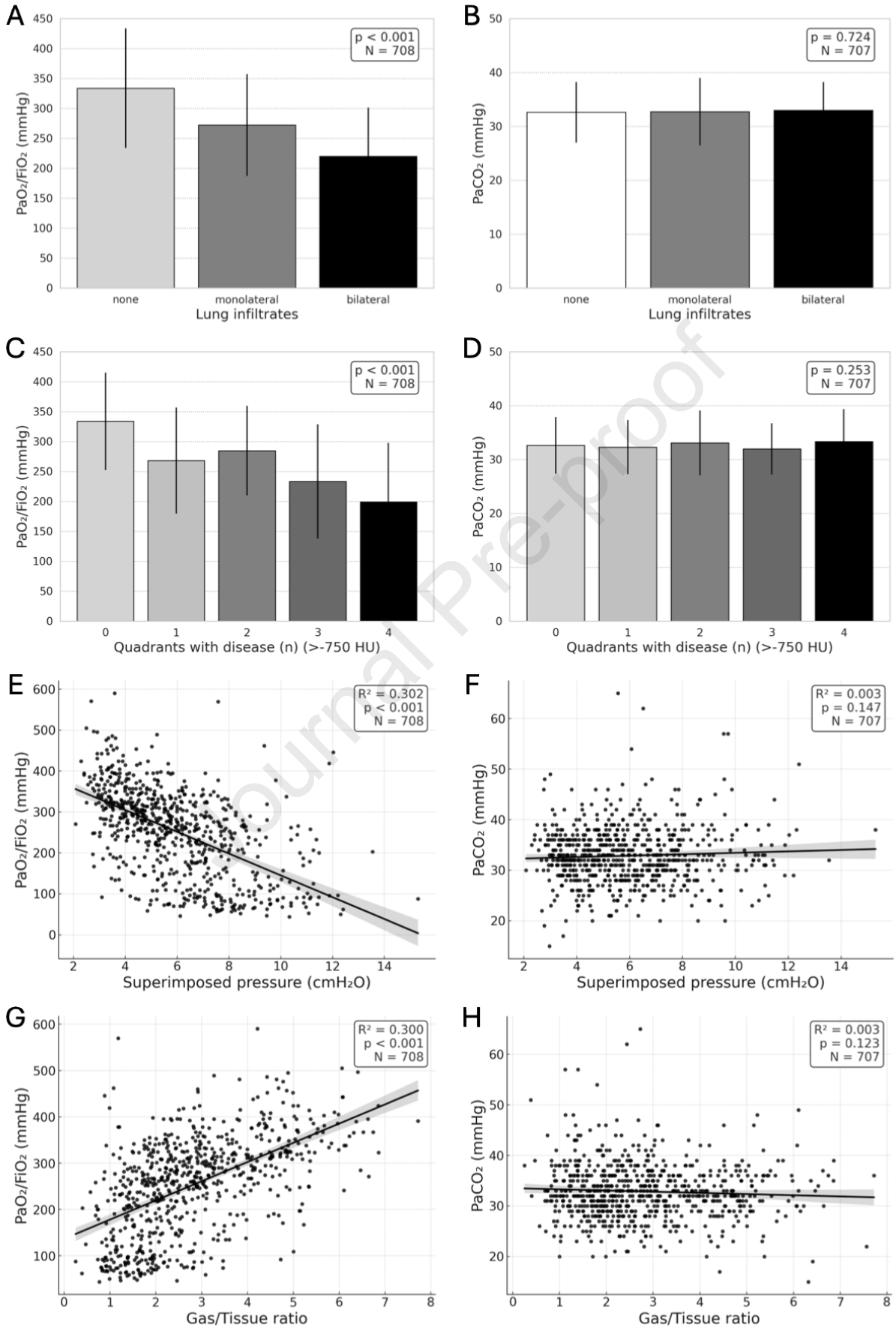
A
p < 0.001
N = 708
PaO₂/FiO₂ (mmHg)
none
monolateral
bilateral
Lung infiltrates
B
p = 0.724
N = 707
PaCO₂ (mmHg)
none
monolateral
bilateral
Lung infiltrates
C
p < 0.001
N = 708
PaO₂/FiO₂ (mmHg)
Quadrants with disease (n) (>-750 HU)
D
p = 0.253
N = 707
PaCO₂ (mmHg)
Quadrants with disease (n) (>-750 HU)
E
R² = 0.302
p < 0.001
N = 708
PaO₂/FiO₂ (mmHg)
Superimposed pressure (cmH₂O)
F
R² = 0.003
p = 0.147
N = 707
PaCO₂ (mmHg)
Superimposed pressure (cmH₂O)
G
R² = 0.300
p < 0.001
N = 708
PaO₂/FiO₂ (mmHg)
Gas/Tissue ratio
H
R² = 0.003
p = 0.123
N = 707
PaCO₂ (mmHg)
Gas/Tissue ratio

Figure 4.